ACS OMEGA

http://pubs.acs.org/journal/acsodf

Article

Computational Screening of Metal–Organic Frameworks for Ammonia Capture from $H_2/N_2/NH_3$ Mixtures

Zhaofan Zhu, Haiou Wang,* Xiao-Yu Wu, Kun Luo, and Jianren Fan

Cite This: *ACS Omega* 2022, 7, 37640–37653

Read Online

ACCESS | Metrics & More | Article Recommendations | Supporting Information

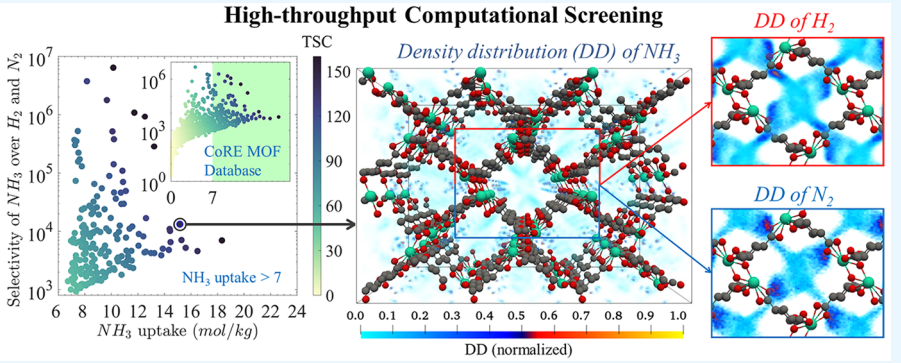

ABSTRACT: The separation of ammonia from $H_2/N_2/NH_3$ mixtures is an important step in ammonia decomposition for hydrogen production and ammonia synthesis from H_2 and N_2 based nonaqueous technologies. Metal–organic frameworks (MOFs) are considered as potential materials for capturing ammonia. In the present work, high-throughput screening of 2932 Computation-Ready Experimental MOFs (CoRE MOFs) was carried out for ammonia capture from $H_2/N_2/NH_3$ mixtures by Grand Canonical Monte Carlo (GCMC) simulations. It was found that the high-performing MOFs are characterized by tube-like channels, moderate LCD (largest cavity diameter) (4–7.5 Å), and high $Q_{st}^0(NH_3)$ (the isosteric heat of NH_3 adsorption) (>45 kJ/mol). MOFs with high NH_3 adsorption capacity often feature moderate surface area, while the surface area of MOFs with high NH_3 selectivity is relatively lower, which limits the NH_3 adsorption capacity. Q_{st}^0 and the Henry's constant (K_H) are two energy descriptors describing the interactions between adsorbents and adsorbates. The former has a stronger correlation with the adsorption selectivity, while the latter has a stronger correlation with the adsorption capacity. By analyzing the molecular density distribution of adsorbates in high-performing MOFs, it was found that unsaturated coordinated metal sites provide the main functional binding sites for NH_3. Most MOFs with high NH_3 selectivity have multiple different metal nodes or other atoms except C, O, and H, such as N and P. Multiple metal nodes and nonmetallic atoms provide more functional binding sites. Finally, the adsorption behavior with various concentrations of gas mixtures was examined to verify the universality of the screening calculations, and the effect of framework flexibility on adsorption performance was explored.

INTRODUCTION

Ammonia (NH_3) is an important chemical in global agriculture and industry as feedstocks for fertilizers, cleaning products, and various drugs, working fluids for heat pumps, and fuels for fuel cells.[1−3] Ammonia can also be used in refrigeration, fermentation, and energy storage and conversion.[4,5] More than 130 million tons of ammonia are produced through the traditional Haber-Bosch process annually to meet the increasing demand from a booming world population and growing industries.[6] This process consumes 2% of the global energy consumption, emits major pollutions,[7] and accounts for about 1.0% of global greenhouse gas emission.[8] Besides, the traditional Haber-Bosch process is not suitable for small-scale operation[6] and therefore cannot be adapted to various flexible distributed applications. Due to the high temperature and high pressure reaction condition required by Haber-Bosch process, the energy loss is relatively high in small-scale operations. Additionally, in the traditional Haber-Bosch process, ammonia is usually separated by condensation, which requires higher energy cost in small-scale operation. In recent years, many green alternative routes for ammonia production have been developed, such as green Haber-Bosch,[9,10] electrochemical synthesis,[11−13] photochemical synthesis,[14−16] electrothermo-chemical looping[17,18] and plasma-enabled synthesis.[19,20] Most

Received: July 18, 2022
Accepted: October 3, 2022
Published: October 10, 2022

of them are carried out at low temperature and atmospheric pressure suitable for small-scale operation, and nonaqueous reactions using N_2 and H_2 as raw materials play important roles in these technologies. For example, the plasma-enabled catalysis ammonia synthesis technology is clean, carbon free, and theoretically energy-efficient and cost-effective.[20] The theoretical energy consumption for nonthermal plasma (NTP) ammonia synthesis has been reported to be about 0.2 MJ/mol,[21] which is lower than that of the Haber-Bosch method (0.48 MJ/mol).[6] The products of these H_2 and N_2 based nonaqueous ammonia synthesis technologies are $H_2/N_2/NH_3$ mixtures, and the capture of NH_3 from the mixtures is an important step to obtain NH_3 and improve the conversion rate of the reaction. In addition, this process also has important significance in ammonia decomposition for hydrogen production, in which NH_3 needs to be separated to obtain pure H_2 or H_2/N_2 mixtures according to anticipated use.[22]

The condensation method used in the traditional Haber-Bosch process does not allow for effective and complete separation at low operating pressures. Therefore, alternative methods for ammonia separation are required for ammonia synthesis under mild pressures. It has been shown that, porous adsorbents are efficient and feasible choices to capture and remove ammonia or separate ammonia from mixtures.[23,24] Porous adsorbents can be operated at relatively low cost under environmental conditions. Currently, solid adsorbents such as zeolite,[25] activated carbon,[26] and metal oxides[27] have attracted widespread attention. As a new type of material, metal−organic frameworks (MOFs) also show great potential.[28]

MOFs are crystalline nanoporous materials assembled from metal nodes and organic linkers. Due to their high surface area, high porosity, controllable pore size, and tunable pore surface,[29,30] MOFs have shown great application potential in gas storage,[31] gas adsorption and separation,[32] catalysis,[33] sensing,[34] and biomedical applications.[35] Ammonia capture by MOFs has received growing research interest due to the ultrahigh surface area, pore volume, and structural diversity that are favorable for selective gas adsorption.[2] It is reported that the groups that can form strong hydrogen bonds with NH_3 can greatly increase the adsorption of NH_3.[36] For example, IRMOF-3 is an amino-functionalized analogue of IRMOF-1 (MOF-5), and its NH_3 adsorption capacity is almost 18 times that of the latter.[37] Khabzina et al.[38] studied the performance of UiO-66-COOH to capture ammonia from air, and showed that its adsorption capacity of NH_3 was higher than that of N_2 under either dry or wet conditions. Yu et al.[39] found that polar group functionalized MOFs have high NH_3 absorption performance at low pressure by molecular simulation. However, due to the large functional groups, the pore volume of the material decreases, and thereby the adsorption capacity decreases under high pressure. Experiments show that MOFs containing open metal sites (OMS) can act as Lewis acid and interact strongly with Lewis base (such as NH_3), so it exhibits very high ammonia absorption capacity.[40]

Although existing studies focus on capturing ammonia from dry or wet air, few were on $H_2/N_2/NH_3$ mixtures. Therefore, we conducted investigations on MOFs for ammonia capture from $H_2/N_2/NH_3$ mixtures for efficient ammonia production and decomposition. With the rapid increasing number of MOFs, there is an urgent need to identify the high-performing candidates for capturing ammonia from $H_2/N_2/NH_3$ mixtures from a large number of MOFs. High-throughput computational screening (HTCS) based on grand canonical Monte Carlo (GCMC) simulations has been used to screen and evaluate high-performing MOFs and explore the relationship between structure and performance. For example, Yuan et al.[41] simulated the adsorption performance of 31399 hydrophobic MOFs for formaldehyde adsorption. They showed the relationship between the structural characteristics of MOFs and formaldehyde adsorption performance, and screened out the high-performing MOFs for formaldehyde adsorption. Liu et al.[42] screened 2932 computation-ready experimental MOFs (CoRE MOFs) and selected excellent MOFs suitable for capturing trace NH_3 from wet air under environmental conditions. In this work, a different HTCS strategy that focuses on the ammonia capture from $H_2/N_2/NH_3$ mixtures was developed, and the adsorption performance of MOFs was computed by GCMC. In particular, we screened out high-performing MOFs from 2932 CoRE MOFs in the CoRE MOFs DDEC Database[43] and analyzed the relationship between structural characteristics and adsorption performance. The remainder of the paper is organized as follows. In the next section, the models and methods are described. Then the results are presented and discussed. Finally, the conclusions are made.

MODELS AND METHODS

Molecular Models. *Models.* Many MOF databases have been published. For example, Wilmer et al.[44] generated all conceivable MOFs from a given chemical library of building blocks (based on the structures of known MOFs), and the structures of the resulting hypothetical MOFs were stored in the hMOF database to provide references for other researchers. The Cambridge Structural Database (CSD) created by the Cambridge Crystallographic Data Centre (CCDC) contains over one million small-molecule organic and metal−organic crystal structures,[45] providing data support for thousands of papers and reviews. Experimentally refined crystal structures for MOFs in CSD often include solvent molecules and partially occupied or disordered atoms. This creates a major impediment to applying high-throughput computational screening to MOFs. To address this problem, Chung et al.[46] constructed a database of CoRE MOF structures that are derived from experimental data and are immediately suitable for molecular simulations (updated in 2019 by the same research group in ref 47). The CoRE MOF database has been widely used for calculation and screening in gas adsorption[48,49] and separation.[50,51] It has been reported that the electrostatic potential plays a leading role in describing the interaction between MOFs and polar gases such as NH_3.[52] Accurate atomic charge of MOFs can describe the electrostatic interaction more accurately. Therefore, in the present work, 2932 CoRE MOFs with high-precision density derived electrostatic and chemical (DDEC) charge[53] from the CoRE MOFs DDEC Database[43] were chosen for simulations for ammonia capture from $H_2/N_2/NH_3$ mixtures.

Force Field Parameter. The adsorption in this work occurs at room temperature and atmospheric pressure conditions. The MOF structures are assumed rigid and all atoms of MOFs are frozen in GCMC simulations. The discussion regarding the effect of framework flexibility will be presented later. Adsorbate−adsorbent and adsorbate−adsorbate interactions were described by van der Waals force and Coulomb force, which are respectively modeled with Lennard-Jones (LJ) potential (eq 1) and Coulomb potential (eq 2):

https://doi.org/10.1021/acsomega.2c04517
ACS Omega 2022, 7, 37640−37653

Table 1. Force Field Parameters of Adsorbates in This Work

Adsorbate	(pseudo) Atom	Type	ε/k_B (K)	σ (Å)	q (e)	source
NH_3	N	[N]-H_3	185.00	3.42	0.000	TraPPE[56]
	H	[H]-NH_2	0	0	0.410	
	com[a]	com-NH_3[a]	0	0	−1.230	
N_2	N	[N]-N	36.00	3.31	−0.482	
	com[a]	com-N_2[a]	0	0	0.964	
H_2	H	[H]-H	38.0	2.915	0.468	ref 57
	com[a]	com-H_2[a]	0	0	−0.936	

[a]com: center-of-mass; com-NH_3, com-N_2 and com-H_2: the center-of-mass of NH_3, N_2 and H_2, respectively.

$$U_{LJ} = 4\epsilon_{ij}\left[\left(\frac{\sigma_{ij}}{r_{ij}}\right)^{12} - \left(\frac{\sigma_{ij}}{r_{ij}}\right)^{6}\right] \quad (1)$$

$$U_{elec} = \frac{q_i q_j}{4\pi\epsilon_0 r_{ij}} \quad (2)$$

where i and j represent the interacting atoms, r_{ij} is the distance between atoms i and j, ε is the depth of potential well, and σ is the equilibrium position of potential energy, q is the atomic charge, and $\varepsilon_0 = 8.8542 \times 10^{-12}$ C^2 N^{-1} is the vacuum permittivity constant.

A spherical cutoff of 14 Å and analytic tail correction were used for the LJ interactions. Electrostatic interactions were computed using the Ewald summation method[54] for both adsorbate−adsorbent and adsorbate−adsorbate interactions. The LJ parameters of all the MOFs were taken from the Universal Force Field (UFF),[55] as listed in Table S1, and DDEC charge[53] was adopted for all atoms of the MOFs. The Transferable Potentials for Phase Equilibria (TraPPE) force field[56] was used for ammonia and nitrogen. The force field parameters for hydrogen were taken from the study of Turner et al.[57] All adsorbate force field parameters are listed in Table 1. The force field parameters between different nonbonded atoms are determined by the Lorentz−Berthelot mixing rule:

$$\sigma_{ij} = \frac{\sigma_{ii} + \sigma_{jj}}{2} \quad (3)$$

$$\epsilon_{ij} = \sqrt{\epsilon_{ii}\cdot\epsilon_{jj}} \quad (4)$$

GCMC Simulation. The void fraction of MOFs is a necessary structural characteristic when simulating the gas adsorption. So before GCMC simulations, the He void fraction (HVF) was computed for all MOFs by RASPA 2.0[58] molecular simulation software, using Widom insertions[59] of a He probe. This mimics how this quantity is measured experimentally using He adsorption, which is used to analyze the relationship between HVF and adsorption performance, the values of which are provided in Table S2. Then the amount adsorbed for NH_3, H_2, and N_2 was calculated using GCMC simulations implemented in the RASPA 2.0.[58] For each cycle in GCMC simulations, the Monte Carlo moves were insertions, deletions, displacements, rotations, and for ternary mixtures of NH_3, H_2, and N_2, identity changes. A cycle is defined as the maximum of 20 or the number of molecules in the system. For each MOF, the full cell contains unit cells, and periodic boundary conditions are applied on the full cell level (not on a unit cell level). The numbers of unit cells in each MOF were adjusted to ensure that the length of each MOF involved in the simulation area in three orthogonal directions is at least twice the LJ cutoff distance.

In order to reduce the computational costs and improve the screening efficiency, we adopted the following strategy. Two rounds of preliminary screening were conducted first and then calculated to equilibrium. The accuracy of this strategy has been proven in previous works.[42,49] In the first round, 1709 MOFs capable of adsorbing NH_3 were screened out by PLD (pore limiting diameter) > 2.6 Å (i.e., the kinetic diameter of NH_3 molecule) and ASA (accessible surface area) > 0 from the 2932 CoRE MOFs. The PLD and ASA of the 2932 CoRE MOFs were calculated using Zeo++[60] by Liu et al.[42] In the second round of preliminary screening, 1×10^4 Monte Carlo cycles including 5×10^3 cycles for equilibration and 5×10^3 cycles for production were used to estimate the gas adsorption performance of the 1709 MOFs. The results, provided in Table S2, were used to evaluate the relationship between structural characteristics of MOFs and adsorption performance. Then, 195 MOFs with ammonia adsorption capacity greater than 7.0 mol/kg were chosen for calculating to equilibrium, in which 4×10^4 Monte Carlo cycles including 2×10^4 cycles for equilibration and 2×10^4 cycles for production were executed. Note that the number of cycles (1×10^4) in the second round of preliminary screening might not be sufficient to achieve converged solutions, so more cycles are added to the 195 MOFs to ensure that equilibrium is reached. The results were provided in Table S3. In addition, Henry's constant (K_H) that reflects the interaction between adsorbates and MOFs was computed for 1709 MOFs at 298 K using the Widom insertion method[59] by RASPA 2.0,[58] which was provided in Table S2.

The operational conditions and gas compositions are listed in Table 2. The temperature and pressure are respectively 298 K and 1 bar, and the molar ratio of N_2 to H_2 is 1:1. According to the optimal value of outlet ammonia concentration in plasma-enabled catalysis ammonia synthesis technology reported by Rouwenhorst and Lefferts,[9] the concentration of NH_3 is 1.0 mol %. To explore the adsorption behaviors of NH_3, H_2, and N_2 in MOFs, the isosteric heat of adsorption (Q_{st}^0) of 1709 MOFs for adsorbates and the gas adsorption density distribution (DD) of several typical MOFs were obtained by RASPA 2.0.[58] The input files and force field files

Table 2. Conditions of GCMC Simulations for Ammonia Capture from $NH_3/H_2/N_2$ Mixtures

Conditions	$NH_3/H_2/N_2$ mixtures		
Temperature (K)	298		
Pressure (Pa)	100000		
Components	NH_3	H_2	N_2
Molar ratio	0.01 (6.943 mg/L)	0.495	0.495

https://doi.org/10.1021/acsomega.2c04517
ACS Omega 2022, 7, 37640−37653

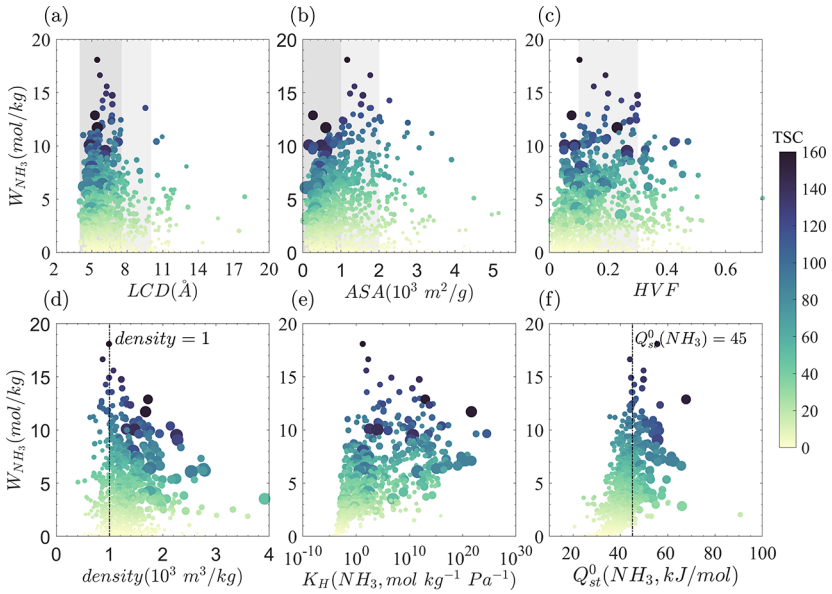

Figure 1. Relationship among (a) LCD, (b) ASA, (c) HVF, (d) framework density, (e) K_H of NH_3, (f) Q^0_{st} of NH_3 and W_{NH_3}, S, and TSC of the 1709 MOFs. The dot size represents S.

for all calculations by RASPA 2.0[58] have been included in the Supporting Information.

The Evaluation Criteria for Ammonia Capture. This work aims to screen out MOFs suitable for capturing NH_3 from $H_2/N_2/NH_3$ mixtures. The target MOFs should have strong adsorption ability for NH_3, while their adsorption ability for H_2 and N_2 should be as weak as possible to improve the selectivity to NH_3. Therefore, MOFs with large NH_3 adsorption capacity and strong NH_3 adsorption selectivity relative to N_2 and H_2 is our focus. After the GCMC simulations, the ammonia selectivity over H_2 and N_2 (S) can be calculated according to the following equation:

$$S = \frac{W_{NH_3}/x_{NH_3}}{W_{H_2+N_2}/x_{H_2+N_2}} \quad (5)$$

where W is the adsorption capacity of adsorbates in MOFs, and x is the mole fraction of adsorbates in the mixtures. Besides, an indicator named trade-off between selectivity and capacity (TSC)[61] was introduced to comprehensively consider the influence of adsorption capacity and adsorption selectivity, and it can be obtained according to the following equation:

$$\mathrm{TSC} = W_{NH_3} \cdot \ln(S) \quad (6)$$

The unit of W_{NH_3} is mol/kg. The TSC was first proposed by Shah et al.[61] in the study of zeolites for the separation of H_2S and CO_2, where the natural logarithm of S is used to achieve a similar order of magnitude with W_{NH_3}. In this work, the ammonia capture performance of MOF was evaluated according to W_{NH_3}, S, and TSC.

RESULT AND DISCUSSION

Structure−Performance Relationship. Yuan et al.[41] studied the relative importance of MOF descriptors by machine learning, and found that ASA, maximum cavity diameter (LCD), K_H, and Q^0_{st} were the four most significant feature descriptors with strong correlations with MOF adsorption performance. HVF and framework density also affect the adsorption performance to some extent. According to the GCMC simulations of 1709 MOFs, four structural descriptors (ASA, LCD, HVF, framework density) and two energetic descriptors (K_H, Q^0_{st}) were selected to further analyze the relationship between the descriptors and the three performance indicators (W_{NH_3}, S, and TSC).

Figure 1 shows the scatter plots of six descriptors of 1709 MOFs and their relationship with three performance indicators. Figure 1a shows that the MOFs with high W_{NH_3} are concentrated in the range of 4 Å < LCD < 10 Å, especially in the range of 4 Å < LCD < 7.5 Å, where the MOFs with high TSC are concentrated. It is worth noting that the shape of pore or channel of MOFs can be described by the ratio of LCD and PLD (i.e., LCD/PLD). The MOFs with tube-like pore morphologies are characterized by LCD/PLD approaching to 1 and MOFs with large cavities connected by narrow channels feature LCD/PLD greater than 1.5. Figure 2 shows the

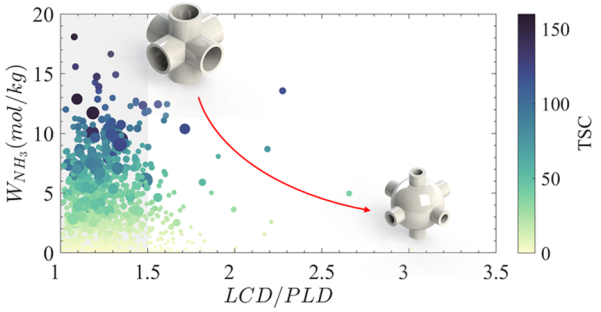

Figure 2. Relationship among LCD/PLD and W_{NH_3}, S, and TSC of the 1709 MOFs. The dot size represents S.

relationship between LCD/PLD and performance indicators of 1709 MOFs. The MOFs with high NH_3 and high TSC are concentrated in the range of 1 < LCD/PLD < 1.5, and the best performance MOFs are at about LCD/PLD = 1.25, which is consistent with the study of Liu et al.[42] The relationship between ASA and performance indicators is shown in Figure

https://doi.org/10.1021/acsomega.2c04517
ACS Omega 2022, 7, 37640−37653

1b. High W_{NH_3} MOFs are concentrated in the range of 1000 < ASA < 2000 m^2/kg, while high S MOFs tend to have smaller ASA than 1000 m^2/kg. Figure 1c indicates that MOFs with high adsorption capacity tend to be in the range of 0.1 < HVF < 0.3, and there is no clear relationship between HVF and adsorption selectivity. Figure 1d shows that the framework density of the MOFs with high adsorption capacity is around 1000 m^3/kg, while that of the MOFs with high adsorption selectivity is generally larger. Figure 1e illustrates the relationship between the energetic descriptor $K_H(NH_3)$ and the performance indicators. K_H reflects the interaction between adsorbates and frameworks. When $K_H(NH_3)$ is too low, the interaction between NH_3 molecules and MOFs is weak, resulting in poor adsorption performance. Figure 1f displays the relationship between another energetic descriptor $Q_{st}^0(NH_3)$ and performance indicators. When $Q_{st}^0(NH_3)$ is too low, there was not a sufficient driving force to promote the adsorption. When $Q_{st}^0(NH_3)$ > 30 kJ/mol, the performance indicators increased significantly with the increase of $Q_{st}^0(NH_3)$, and the maximum TSC appeared in $Q_{st}^0(NH_3)$ > 45 kJ/mol, which is in line with the results reported by Qiao et al.[62] for the capture of low concentration thiol from the air.

In summary, MOFs with good adsorption performance have tube-like pore morphologies, along with LCD in the range of 4−7.5 Å, and $Q_{st}^0(NH_3)$ > 45 kJ/mol. The ASA of MOFs with high W_{NH_3} is in the range of 1000−2000 m^2/kg, while the ASA of MOFs with high S is smaller. Figure 1 qualitatively shows the distribution of high-performing MOFs, but it cannot explain the relationship between MOF descriptors and performance indicators, which needs to be further explored by statistical methods.

As shown in Figure 3, 1709 MOFs were classified into four categories, i.e., types A, B, C, and D, according to the

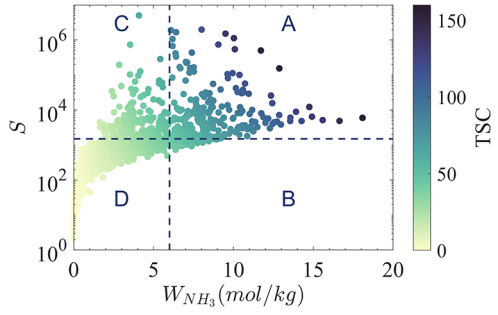

Figure 3. Classification of MOFs according to W_{NH_3} and S.

thresholds of W_{NH_3} = 6 mol/kg and S = 1500. These two critical values were chosen to distinguish high-performing MOFs and ensure that each category has a sufficient number of MOFs. The relationship between MOF descriptors and adsorption performance is analyzed based on the statistical results shown in Figure 4. In general, most samples of type A (high W_{NH_3} and high S) exhibit tube-like channels (1 < LCD/PLD < 1.3), moderate LCD (5−7.5 Å), moderate HVF (0.1−0.31), high $Q_{st}^0(NH_3)$ (>40 kJ/mol) and wide ASA distribution (0−2500 m^2/kg).

The proportions of high $K_H(NH_3)$ in types A and B are significantly higher than those in types C and D, and the proportions of high $Q_{st}^0(NH_3)$ in types A and C are significantly higher than those in types B and D. As types A and B have higher W_{NH_3}, while types A and C have higher S, it can be deduced that K_H has a stronger correlation with NH_3 adsorption capacity, while Q_{st}^0 has a stronger correlation with NH_3 adsorption selectivity.

Compared with types B and D, types A and C have higher proportions of low LCD/PLD and low ASA. As shown in Figure 1b and Figure 2, the high S MOFs tend to appear in the left regions near the ordinate axes in Figure 1b and Figure 2. The reason was speculated to be that MOFs with small ASA contain pore channels (i.e., the LCD/PLD is small), which allowed NH_3 molecules to contact the pore walls of the MOFs intimately. Conversely, when the ASA is too large, the adsorption volume and the number of adsorption sites of H_2 and N_2 as the main parts of the mixed gas increased, and the relative contact area between the pore walls and NH_3 decreased with the increasing ASA. This tends to limit the adsorption of NH_3. Therefore, low LCD/PLD and low ASA (exhibit tube-like pore morphologies) are beneficial to highly selective adsorption of NH_3. Liu et al.[42] drew similar conclusions in the study of NH_3 capture from wet air. On the other hand, the proportion of moderate LCD in types A and B is significantly higher than that in types C and D. Figure 1a shows that when the LCD < 4 Å, the steric hindrance between the NH_3 molecules and hole walls limited the adsorption of the frameworks. When LCD > 7.5 Å, the interactions between the frameworks and NH_3 molecules decreased, which intensified the desorption of NH_3 in the pores and reduced the adsorption capacity. High W_{NH_3} MOFs are more likely to be found in the moderate LCD range (5−7.5 Å).

Compared with types C and D, types A and B have higher proportions of moderate HVF (0.1−0.31). Figure 1c shows that when the HVF is <0.04 or >0.31, the adsorption capacity of MOFs decreased significantly. When HVF is too small, the available adsorption volume limits the adsorption of NH_3. However, with large HVF, the relative surface area reduces, and hence, less adsorption sites are available. This leads to a drop in W_{NH_3}. In addition, the high framework density accounts for a large proportion in type C (high S and low W_{NH_3}). As shown in Figure 1d, a certain framework density can ensure that MOFs have sufficient adsorption sites, but for excessively dense MOFs, the forces between the MOFs and NH_3 molecules change from attraction to repulsion, hindering the adsorption effects.

High-Performing MOFs after Screening. As shown in Figure 5, in the above screening calculation, 195 MOFs were finally selected to calculate to equilibrium. The average W_{NH_3} deviation of these 195 MOFs between the preliminary screening and final screening is 2.70%, and most of the deviation is within 6%. As shown in Figure 5a, the adsorption capacity obtained from the preliminary screening and that from equilibrium calculation is relatively consistent. Therefore, it is reliable and accurate to evaluate the structure−performance relationship with the preliminary screening results of 1709 MOFs. The 195 MOFs were first sorted by TSC obtained from equilibrium calculations, and the top 20 high TSC MOFs were listed in Table 3. It is shown that most of the top high TSC MOFs have either high W_{NH_3} or S, indicating that TSC reflects the balance between adsorption capacity and selectivity to a certain degree. Then, the 195 MOFs were also sorted according to W_{NH_3} and S obtained from equilibrium calculation, and the top 20 MOFs with the highest W_{NH_3} and

https://doi.org/10.1021/acsomega.2c04517
ACS Omega 2022, 7, 37640−37653

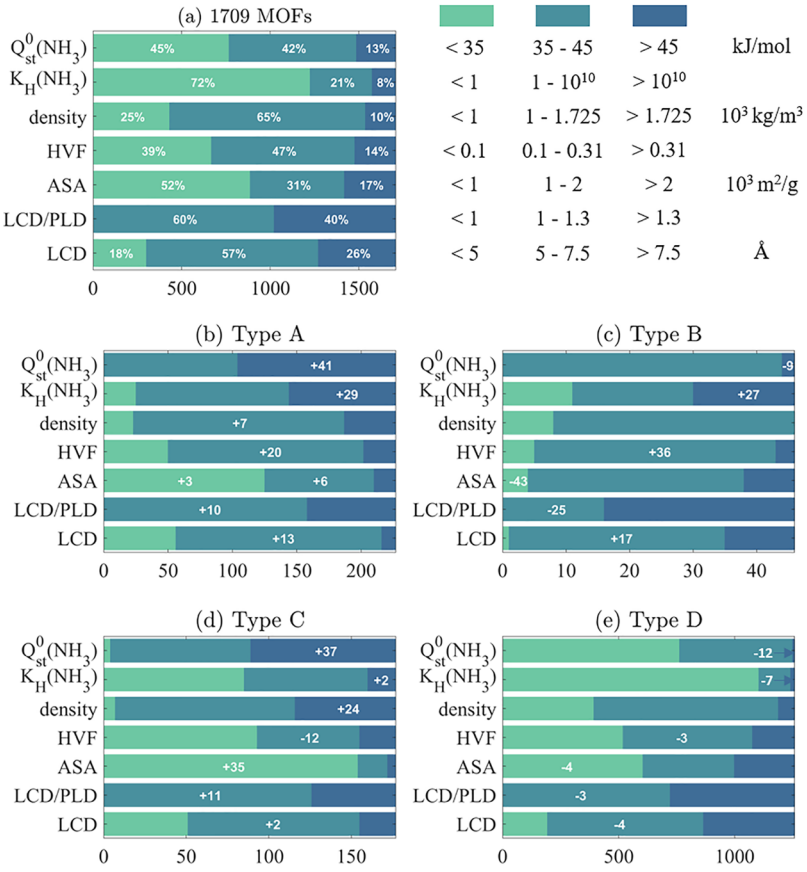

Figure 4. Distribution of descriptors in different ranges for (a) 1709 MOFs, (b−e) types A, B, C, D MOFs; the numbers in (a) represent the percentage of MOFs in different ranges of descriptors, and the numbers in (b−e) represent the percentage change from the percentage in (a).

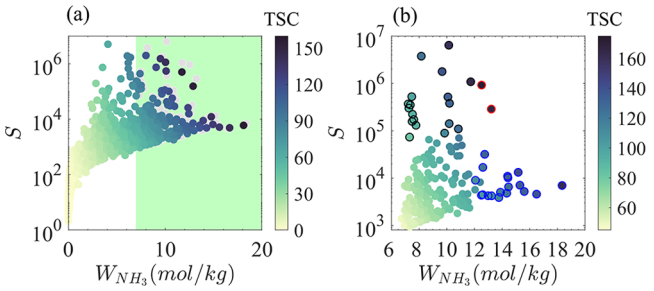

Figure 5. Relationship among W_{NH_3} and S in (a) 1709 MOFs in preliminary screening, (b) 195 MOFs in final screening. The MOFs with W_{NH_3} > 7 mol/kg in (a) are highlighted by green shading. The gray dots are the projection of (b) on (a). The top 20 high-W_{NH_3} MOFs, top 20 high-S MOFs, and their overlapping parts in (b) are highlighted by blue, black, and red edges, respectively.

S are summarized in Tables 4 and 5, respectively. Most of these MOFs are in the optimal ranges discussed above, except for KEVWUF in the high W_{NH_3} group. The W_{NH_3} of KEVWUF is as high as 14.46 mol/kg, but the LCD/PLD is 2.27, much higher than the optimal range (1−1.5). To explore the adsorption behaviors of adsorbates in KEVWUF, the gas adsorption density distribution was calculated by RASPA 2.0[58] and visualized by ParaView,[63] as shown in Figure 6a. It can be observed that NH_3 is mainly adsorbed around metal sites. In the region away from the framework, NH_3 is uniformly distributed, where the interaction between NH_3 and pore walls is weak due to the large pore size. It is speculated that the high

Table 3. Rankings by W_{NH_3} and S (i.e., rank-W_{NH_3} and rank-S, respectively) of the Top 20 High TSC MOFs

rank-TSC	ref code	rank-W_{NH_3}	rank-S
1	GEVXIQ	18	5
2	VODSEM	13	12
3	XECJUK	23	4
4	OSAVEK	1	79
5	HEDBOJ	58	1
6	COWMAD	5	45
7	HEDBUP	67	3
8	VAGTAA	2	102
9	BEXSAA	4	78
10	COWMUX	8	54
11	NOCLUN	3	92
12	COWMIL	7	57
13	UFOFIF	60	7
14	FALVOF	15	30
15	TEHRUU	55	8
16	KEVWUF	6	82
17	WASVES	39	18
18	COXXIX	120	2
19	WIYZOU	16	43
20	XEKCAT01	9	98

W_{NH_3} of KEVWUF is caused by the strong interaction between metal site La and NH_3 molecules.

Comparing MOFs with high W_{NH_3} and high S, it is found that the ASA of high S MOFs is significantly lower than that of

https://doi.org/10.1021/acsomega.2c04517
ACS Omega 2022, 7, 37640−37653

Table 4. Structural Characteristics and Adsorption Performance of the Top 20 High W_{NH_3} MOFs

rank-W_{NH_3}	ref. code	Molecular formula	LCD[a] (Å)	LCD/PLD	ASA[a] (m^2/g)	HVF	density (kg/m^3)	K_H of NH_3 (mol kg^{-1} Pa^{-1})	WNH3 (mol/kg)	S	rank-TSC
1	OSAVEK	$CaH_4(C_2O)_4$	5.46	1.08	1165	0.10	991.06	1.74×10^{1}	18.33	6.98×10^{3}	4
2	VAGTAA	$MgH_4(C_4O_3)_2$	5.69	1.29	1771	0.19	871.91	1.88×10^{2}	16.49	4.59×10^{3}	8
3	NOCLUN	$SrH_4(C_2O)_4$	6.27	1.09	1356	0.15	1074.04	8.08×10^{1}	15.60	5.22×10^{3}	11
4	BEXSAA	$Mn_3H_{16}C_{30}(NO_7)_2$	6.22	1.32	1240	0.20	992.36	4.13×10^{6}	15.29	7.09×10^{3}	9
5	COWMAD	$DyH_9(C_3O_2)_3$	6.74	1.21	1578	0.30	1222.61	7.13×10^{11}	15.16	1.33×10^{4}	6
6	KEVWUF	$LaH_3C_7NO_4$	9.54	2.27	1789	0.28	1041.67	1.30×10^{8}	14.46	6.52×10^{3}	16
7	COWMIL	$HoH_9(C_3O_2)_3$	6.74	1.22	1529	0.30	1237.90	3.57×10^{10}	14.42	1.02×10^{4}	12
8	COWMUX	$TmH_9(C_3O_2)_3$	6.71	1.21	1525	0.29	1259.57	1.05×10^{11}	14.39	1.10×10^{4}	10
9	XEKCAT01	$MgH_2(C_3O_2)_2$	5.92	1.20	2275	0.24	930.33	3.02×10^{4}	14.33	4.80×10^{3}	20
10	KAYCIY	$CaH_3C_7NO_4$	5.92	1.22	1754	0.20	976.74	9.88×10^{1}	13.88	5.03×10^{3}	24
11	ETEJIX01	$LaH_2(C_4O_3)_3$	6.70	1.40	2058	0.25	1058.36	2.27×10^{12}	13.76	3.89×10^{3}	26
12	AWOFOI	$CeH_3(C_3O_2)_3$	5.45	1.30	1321	0.13	1318.71	8.68×10^{11}	13.24	4.23×10^{3}	31
13	VODSEM	LaC_5O_6	5.27	1.09	265	0.08	1723.34	9.51×10^{12}	13.22	2.87×10^{5}	2
14	NIGFUF	$DyH_3(C_3O_2)_3$	7.46	1.61	1880	0.28	1230.05	2.81×10^{14}	12.99	4.24×10^{3}	36
15	FALVOF	$Pr_2Cu_2H_5(C_5O_4)_5$	6.66	1.47	1072	0.27	1393.37	5.79×10^{13}	12.74	3.18×10^{4}	14
16	WIYZOU	$Co_5H_2(C_{11}O_{10})_2$	6.70	1.56	1037	0.30	1328.84	9.62×10^{4}	12.61	1.68×10^{4}	19
17	QAQRUW	$MgH_6(C_3O)_4$	6.66	1.43	2012	0.19	851.39	1.38×10^{6}	12.60	4.47×10^{3}	38
18	GEVXIQ	$Gd_2H_3(C_5O_4)_3$	5.47	1.19	604	0.23	1678.16	4.37×10^{21}	12.52	9.20×10^{5}	1
19	QAQRUW01	$MgH_6(C_3O)_4$	6.66	1.43	2012	0.19	851.39	3.05×10^{4}	12.50	4.35×10^{3}	39
20	LEVNOQ	$MgH_6(C_3O)_4$	5.91	1.50	1207	0.10	974.55	1.47×10^{5}	12.41	8.19×10^{3}	29

[a]The LCD and ASA were calculated using a probe with the nitrogen radius of 1.82 Å in Zeo++ 0.3, from ref 42.

Table 5. Structural Characteristics and Adsorption Performance of the Top 20 High S MOFs

rank-S	ref. code	Molecular formula	LCD[a] (Å)	LCD/PLD	ASA[a] (m^2/g)	HVF	density (kg/m^3)	K_H of NH_3 (mol kg^{-1} Pa^{-1})	W_{NH_3} (mol/kg)	S	rank-TSC
1	HEDBOJ	$CeU_2C_{12}O_{13}$	6.13	1.35	602.08	0.26	2258.84	4.47×10^{10}	10.15	6.39×10^{6}	5
2	COXXIX	$Mn_2Mo(CN)_8$	5.00	1.28	427.97	0.11	1443.68	1.96×10^{1}	8.16	3.75×10^{6}	18
3	HEDBUP	$NdU_2C_{12}O_{13}$	6.08	1.34	591.49	0.26	2279.13	1.76×10^{10}	9.67	1.77×10^{6}	7
4	XECJUK	$SrH_2C_6(NO_2)_2$	4.90	1.18	480.46	0.09	1468.32	1.00×10^{4}	11.73	1.08×10^{6}	3
5	GEVXIQ	$Gd_2H_3(C_5O_4)_3$	5.47	1.19	603.66	0.23	1678.16	4.37×10^{21}	12.52	9.20×10^{5}	1
6	BAXSIE	$Mg_2H_2C_5N_2O_5$	5.31	1.05	498.28	0.07	1498.96	1.42×10^{2}	7.47	5.24×10^{5}	44
7	UFOFIF	$Mn_2NbH_4(C_6N_5)_2$	4.79	1.31	156.71	0.05	1318.06	3.24×10^{2}	10.09	5.17×10^{5}	13
8	TEHRUU	$Nd_2Ru_3H_6(C_4N_3)_6$	4.78	1.31	254.78	0.05	1552.76	3.42×10^{13}	10.20	3.79×10^{5}	15
9	TEJGIA01	$SmH_4C_7(NO_3)_2$	4.65	1.21	343.90	0.07	1879.64	3.65×10^{20}	7.22	3.69×10^{5}	58
10	FATKIW	$SmH_4C_7(NO_3)_2$	4.93	1.33	341.75	0.07	1891.55	4.57×10^{21}	7.37	3.51×10^{5}	52
11	TEJGIA	$SmH_4C_7(NO_3)_2$	4.64	1.20	351.18	0.07	1882.85	6.36×10^{19}	7.26	3.00×10^{5}	60
12	VODSEM	LaC_5O_6	5.27	1.09	264.58	0.08	1723.34	9.51×10^{12}	13.22	2.87×10^{5}	2
13	KESHAT	$PrH_4C_7(NO_3)_2$	4.71	1.21	418.14	0.07	1787.76	7.97×10^{16}	7.53	2.23×10^{5}	57
14	TARVOX	$CoH(C_2N_3)_3$	4.84	1.11	364.15	0.16	1561.14	$1.41 \times 10^{\circ}$	7.62	1.72×10^{5}	59
15	VIPYOK	$Mn_2H_5C_9N_5O_6$	4.56	1.17	354.23	0.09	1544.24	3.23×10^{2}	7.50	1.57×10^{5}	67
16	YISFEL	$Sr_2Cu(CO_2)_6$	5.46	1.29	285.76	0.08	1768.27	9.78×10^{5}	10.18	1.41×10^{5}	22
17	FATKUI	$CeH_4C_7(NO_3)_2$	4.72	1.21	431.41	0.07	1764.11	4.79×10^{19}	7.78	1.30×10^{5}	61
18	WASVES	$La_4Mo_{12}PH_2(C_5O_{18})_2$	7.25	1.71	653.43	0.42	2143.28	1.04×10^{16}	10.84	1.09×10^{5}	17
19	NIBXUT	$Gd_3P_4H_8(CO_3)_8$	6.21	1.20	661.56	0.33	1938.65	3.36×10^{24}	9.85	8.90×10^{4}	28
20	TARVUD	$NiH(C_2N_3)_3$	5.53	1.09	430.82	0.16	1574.98	2.00×10^{-1}	7.32	7.33×10^{4}	87

[a]The LCD and ASA were calculated using a probe with the nitrogen radius of 1.82 Å in Zeo++ 0.3, from ref 42.

high W_{NH_3} MOFs. Note that MOFs with small ASA contain pore channels,[41] whose NH_3 adsorption selectivity is high because NH_3 molecules are closely contacted with the pore walls of MOFs, which is consistent with the above discussion. The NH_3 adsorption selectivity of high W_{NH_3} MOFs is relatively low. However, the higher ASA provides a larger adsorption area, so the NH_3 adsorption capacity is significantly higher than that of high S MOF. To investigate the adsorption behaviors of adsorbates in high-performing MOFs, we selected some typical MOFs (COWMAD, NOCLUN, and NIBXUT) from high W_{NH_3} MOFs and high S MOFs, the gas adsorption density distribution of which were calculated by RASPA 2.0[58] and visualized by ParaView,[63] as shown in Figure 6b−d. Besides, a typical MOF (DIDBEZ) with poor performance was selected as a comparison as shown in Figure 6e.

In COWMAD, the adsorption intensity of NH_3 is the largest near the metal sites, followed by near linkers, and the pore centers away from the frameworks is the weakest. The adsorption of NH_3 in NOCLUN and NIBXUT also showed the same trend. It can be speculated that metal sites provide the main adsorption sites of NH_3. For H_2 and N_2, there are regions of slightly high adsorption intensity near the metal sites

https://doi.org/10.1021/acsomega.2c04517
ACS Omega 2022, 7, 37640−37653

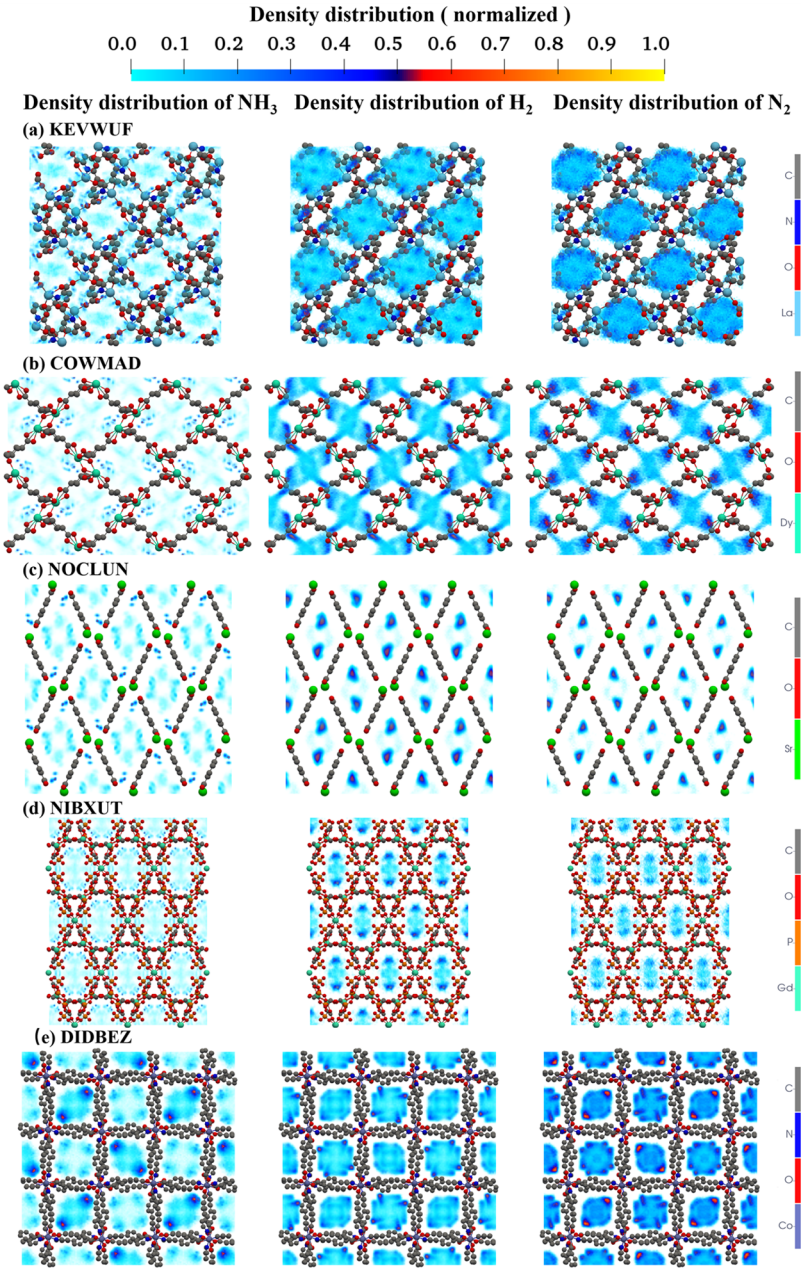

Figure 6. Density distribution maps of NH_3, H_2, and N_2 adsorption in (a) KEVWUF, (b) COWMAD, (c) NOCLUN, (d) NIBXUT, and (e) DIDBEZ.

Table 6. Structural Characteristics and Adsorption Performance of DIDBEZ

ref code	Molecular formula	LCD[a] (Å)	LCD/PLD	ASA[a] (m^2/g)	HVF	density (kg/m^3)	K_H of NH_3 (mol kg^{-1} Pa^{-1})	W_{NH_3} (mol/kg)	S	rank-TSC
DIDBEZ	$CoH_{16}C_{24}(NO_2)_2$	9.18	1.54	1452.45	0.17	928.50	1.13×10^{-4}	0.13	19.71	1233

[a]The LCD and ASA were calculated using a probe with the nitrogen radius of 1.82 Å in Zeo++ 0.3, from ref 42.

in COWMAD, while the main adsorption regions are uniformly dispersed in pores. In NOCLUN, the adsorption sites of H_2 and N_2 are concentrated in the pore center far from the pore walls, and the closer to the pore center, the higher the adsorption intensity, which may be caused by the strong interaction resulting from overlapped well depth in its small pore size. The adsorption of H_2 and N_2 in NIBXUT was similar to that in COWMAD, but high adsorption intensity appears in narrow regions in pores, not near metal sites, which may be due to the superposition of the pore wall-adsorbate interaction in the narrow regions. The three different adsorption characteristics are presumed to be caused by the different pore structures and interaction strengths between metal sites and H_2, N_2 in different MOFs.

The low ASA and high framework density of high S MOFs limit the adsorption area and adsorption volume of gas molecules, thereby reducing the adsorption capacity of NH_3, H_2, and N_2. At the same time, the high S MOFs have very high

https://doi.org/10.1021/acsomega.2c04517
ACS Omega 2022, 7, 37640−37653

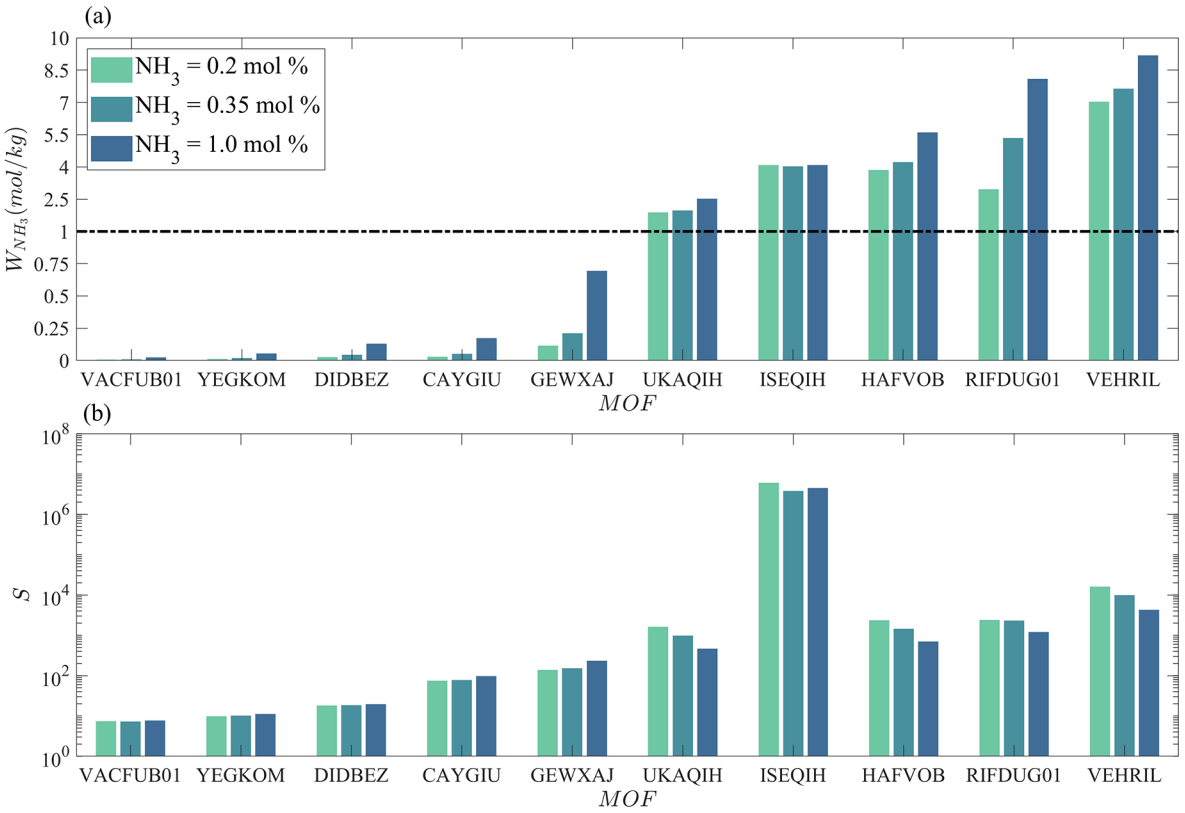

Figure 7. Adsorption performance of 10 MOFs at different NH_3 concentrations and N_2/H_2 = 1:1, (a) W_{NH_3}, (b) S; the ordinate of (a) is scaled with the dot-dash line as the boundary.

K_H for NH_3, which makes a certain compensation for the limitation of ASA and framework density on adsorption capacity. It can be noticed from molecular formulas and structures of MOFs that most high S MOFs have multiple different metal nodes or other atoms except C, O, and H, such as N and P. A variety of metal nodes and nonmetallic atoms provide more adsorption sites, and their interaction with NH_3 molecules may be the main reason for high $K_H(NH_3)$ and high S. Comparing the gas adsorption density distribution of NIBXUT with COWMAD and NOCLUN, the P atom in NIBXUT played this role.

The structural parameters and adsorption performance of DIDBEZ are summarized in Table 6 for comparison. The W_{NH_3} of DIDBEZ is only 0.132 mol/kg, which is much lower than that of high W_{NH_3} MOFs and high S MOFs. In addition, the adsorption capacities of H_2 and N_2 are 0.245 mol/kg and 0.416 mol/kg, respectively. The adsorption capacity of NH_3 is smaller than that of H_2 and N_2 because of its low gas concentration. The distribution of NH_3, H_2, and N_2 adsorption density of DIDBEZ shows similar characteristics. There are regions with high adsorption intensity in the pore corner, and the main adsorption regions are evenly dispersed in pores, which is related to the large LCD of DIDBEZ and the special pore structure. The LCD of DIDBEZ is 9.18 Å, much higher than the optimal range (4−7.5 Å). Due to the large pores, the relative contact area between gas molecules and pore walls is small, and the interaction between pore walls and gas molecules has little effect on the adsorption performance. Due to the superposition of the effects of adjacent organic ligands, the high adsorption intensity regions are generated at the pore corner. It can be speculated that unsaturated coordinated metal sites, such as Dy in COWMAD, Sr in NOCLUN, and Gd in NIBXUT, can interact strongly with NH_3, but saturated coordinated metal sites cannot, such as Co in DIDBEZ. This is in line with the experimental results of Bobbitt et al.[40] Unsaturated coordinated metal sites, i.e.. open metal sites, play an important role in ammonia capture. MOFs containing open metal sites acting as Lewis acid exhibit high ammonia absorption capacity.

Kajiwara et al.[64] found that the ammonia adsorptive behavior of MOFs is independent of their stability against ammonia. However, the stability of MOFs to this corrosive gas must be considered when they are applied in technologies that require thousands of adsorption cycles.[65] The stability of MOFs against ammonia has been investigated experimentally by comparing their power X-ray diffraction (PXRD) patterns before and after treatment with ammonia.[64,66] For example, Liu et al.[66] experimentally obtained the PXRD of NU-1000 and MIL-101, and the change curves of the adsorption capacity in the cycling experiments to investigate the ammonia stability of NU-1000 and MIL-101. Using this method, Kajiwara et al.[64] found that MOFs composed of the combination of oxophilic metal cations and oxygen donors as organic linkers show high stability against ammonia, and MOFs with labile metal cations are more reactive with ammonia than those possessing inert metal cations. The stability of MOFs against ammonia is an important criterion to determine whether they can be used in practice. In this work, MOFs with application potential for ammonia capture from $H_2/N_2/NH_3$ mixtures are screened out without considering their stability, and in the follow-up research, we will conduct experiments to explore the stability of the screened MOFs.

https://doi.org/10.1021/acsomega.2c04517
ACS Omega 2022, 7, 37640−37653

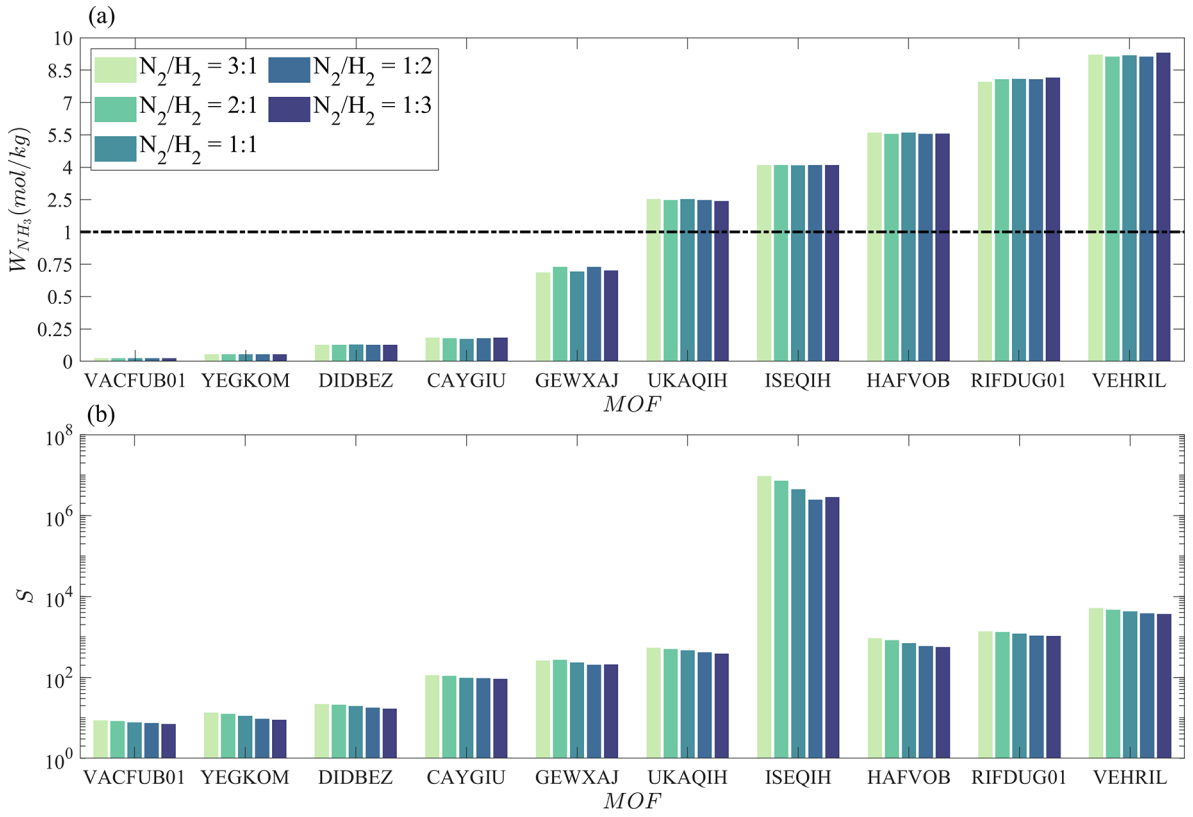

Figure 8. Adsorption performance of 10 MOFs at a NH_3 concentration of 0.2 mol % and different molar ratios of N_2 and H_2, (a) W_{NH_3}, (b) S; the ordinate of (a) is scaled with the dot-dash line as the boundary.

Adsorption Performance at Different Gas Concentrations. The concentration of NH_3 used in the above simulations is 1.0 mol %, which is the optimal value of outlet ammonia concentration in plasma-enabled catalysis ammonia synthesis technology at room temperature and atmospheric pressure reported by Rouwenhorst and Lefferts,[9] taking into account the energy consumption of the reaction gas cycle and the cost of product separation. The current best reported value of energy consumption is 95 GJ/t-NH_3 at a outlet NH_3 concentration of 0.2 mol %. According to the existing research, Rouwenhorst and Lefferts[9] predicted that the energy consumption decreases to the expected value of 80 GJ/t-NH_3 (40 GJ/t-NH_3 for the recycle) at a outlet NH_3 concentration of 0.35 mol %. In addition to the uncertainty of the NH_3 outlet concentration, the molar ratio of N_2 and H_2 used in ammonia synthesis reactions also has different choices. There are many different molar ratios of N_2 and H_2 in current reports. For example, Wang et al.[20] carried out plasma-enabled catalysis ammonia synthesis on Ni/Al_2O_3 catalyst at near room temperature with the molar ratio of N_2 and H_2 of 1:2, and obtained an outlet NH_3 concentration of 0.68 mol %. Peng et al.[67] tested the molar ratios of N_2 and H_2 at 5:1, 4:1, 3:1, 2:1, 1:1, 1:2, and 1:3, and found that the highest ammonia yield was obtained at 3:1.

In order to explore the effects of different NH_3 concentrations and different molar ratios of N_2 and H_2 on the adsorption performance of MOFs, 1709 MOFs were sorted according to W_{NH_3}, and 10 MOFs were selected by equivalent deviations. The adsorption performance of these 10 MOFs under different conditions was simulated. First, considering the molar ratio of N_2 and H_2 being 1:1, and NH_3 concentration being 0.2 mol %, 0.35 mol %, and 1.0 mol %, the adsorption performance of 10 MOFs under different NH_3 concentrations is shown in Figure 7. Then, considering the NH_3 concentration being 1.0 mol %, molar ratio of N_2 and H_2 being 3:1, 2:1, 1:1, 1:2, and 1:3, the adsorption performance of 10 MOFs under different molar ratios of N_2 and H_2 is shown in Figure 8. It can be observed from Figure 7 and Figure 8 that the S of ISEQIH is significantly higher than that of other MOFs, but its W_{NH_3} does not have the corresponding outstanding performance. The main reason is that the ASA of ISEQIH is only 320 m^2/g, and low ASA is more conducive to high S, but W_{NH_3} is limited by low ASA, which is consistent with the above discussion. It can be observed from Figure 7 that NH_3 concentration has a small effect on W_{NH_3} and S. When NH_3 concentration is high, W_{NH_3} is generally larger, and the effect of NH_3 concentration on S value is not obvious. Because of the large pore size of RIFDUG01 (LCD = 13 Å), its adsorption performance is slightly different from those of other MOFs. The large adsorption volume makes a great contribution to the adsorption capacity, so W_{NH_3} is greatly affected by NH_3 concentration. It can be observed from Figure 8 that the molar ratio of N_2 to H_2 has little effect on W_{NH_3} and S. The adsorption performance of MOFs for gas molecules depends on the interaction between the two, and is also affected by the pore size, accessible surface area, porosity, and other structural characteristics of MOFs. The former is determined by the characteristics of MOFs and adsorbates, and the latter is the inherent property of MOFs. Therefore, the gas concentration has little effect on the NH_3 capture performance of MOF,

https://doi.org/10.1021/acsomega.2c04517
ACS Omega 2022, 7, 37640−37653

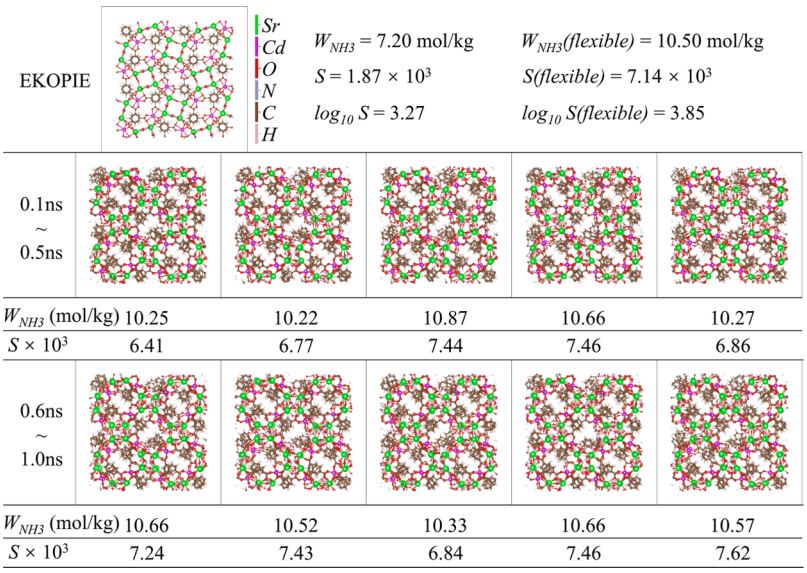

Figure 9. The initial structure of EKOPIE and 10 snapshots obtained during NVT MD simulation, along with the W_{NH_3} and S calculated using each structure, W_{NH_3} (flexible) and S(flexible) are adsorption capacity of ammonia and adsorption selectivity allowing intrinsic flexibility, respectively.

which reflects that the screening in this work has certain universality for NH_3 capture from $H_2/N_2/NH_3$ mixtures.

Effect of Framework Flexibility on Selective Adsorption of NH_3. In the above analysis, MOFs are assumed stable during the physical adsorption process, and all atoms of MOFs are frozen in the GCMC simulations. This assumption was widely used in screening calculations and provides excellent prediction results.[41,42,49,50,62] However, MOFs are highly flexible. Some researchers have explored the influence of framework flexibility of MOFs on the adsorption performance.[68−70] For example, Park et al.[68] investigated the impact of framework flexibility on selective adsorption of sarin using MOFs, and they found that modeling the MOFs as rigid tends to underestimate the adsorption selectivity.

In order to understand the effect of framework flexibility on the absorption characteristics, we chose one representative MOF from the 1709 MOFs, i.e., EKOPIE, and examined the adsorption performance of this MOF allowing intrinsic flexibility. The flexible snapshot method proposed by Gee and Sholl[69] was used to generate an ensemble of empty MOF frameworks by simulating the dynamics of the MOF.[70] Canonical ensemble (NVT) molecular dynamics (MD) simulation was conducted after structure relaxation and NVT MD snapshots that represent intrinsically flexible empty MOF were generated. Then independent GCMC simulations were performed by RASPA 2.0[58] using various MOF structures taken from MD snapshots. The framework charges were calculated via charge equilibration proposed by Wilmer and Snurr.[71] Each structure was kept rigid during these GCMC simulations. The adsorption data were then averaged over GCMC results from each MD snapshot. The NVT MD simulation was performed in LAMMPS[72] at 298 K with a time step of 1.0 fs. The temperature was controlled via a Nosé−Hoover thermostat with a 0.1 ps decay period. Each MOF was described using the UFF4MOF force field proposed by Coupry et al.[73] The simulation includes an equilibration period of 500 ps and a production period of 1 ns. Snapshots from the simulation were taken every 100 ps from the production period for a total of 10 snapshots. The adsorption data were obtained based on the 10 snapshots. Previous work by Agrawal and Sholl[70] and Park et al.[68] showed that this was sufficient to achieve converged results. The input files for NVT MD and GCMC simulations have been included in the Supporting Information, and the adsorption performance for each structure was provided in Table S4.

Figure 9 shows the initial structure of EKOPIE and the 10 snapshots obtained during NVT MD simulation, along with the W_{NH_3} and S calculated using each structure. The adsorption capacity of each gas component allowing intrinsic flexibility is the average of the adsorption capacities of 10 snapshots, and the selectivity is calculated according to adsorption capacity by eq 5. Compared with rigid EKOPIE, both W_{NH_3} and S are higher in flexible EKOPIE, and the increased selectivity in the flexible EKOPIE is associated with higher adsorption capacity of NH_3 and lower adsorption capacity of H_2 and N_2 than in the rigid EKOPIE. This result is consistent with the conclusion of Park et al.[68] Therefore, the intrinsic flexibility of MOFs cannot be ignored in pursuit of precise results on the adsorption performance. However, the assumption that MOFs are rigid is still useful in high-throughput computational screening, because the purpose of the screening is to identify a batch of potential MOFs.

CONCLUSIONS

In the present work, in order to identity high-performing MOFs for ammonia capture from $H_2/N_2/NH_3$ mixtures, 2932 CoRE MOFs were assessed using high-throughput computational screening based on GCMC simulations. It was found that high-performing MOFs exhibit tube-like channels (1 < LCD/PLD < 1.5), moderate LCD (4−7.5 Å), and high $Q_{st}^0(NH_3)$ (>45 kJ/mol). The ASA of high W_{NH_3} MOFs is in the range of 1000−2000 m^2/kg, while that of high S MOFs is smaller. Classification of MOFs based on both their ammonia capacity and selectivity demonstrated that Q_{st}^0 and K_H are two energy descriptors describing the interactions between adsorbents and adsorbates, with the former having a stronger correlation with the adsorption selectivity, while the latter has a stronger correlation with the adsorption capacity. Low LCD/PLD and low ASA are conducive to obtaining high adsorption

https://doi.org/10.1021/acsomega.2c04517
ACS Omega 2022, 7, 37640−37653

selectivity, and medium HVF is conducive to obtaining high adsorption capacity. MOFs with high framework density tend to have high selectivity and low adsorption capacity.

The screening resulted in 20 high W_{NH_3} MOFs and 20 high S MOFs. It was found that unsaturated coordinated metal sites, i.e., open metal sites, provide the main adsorption sites of NH_3 from the gas adsorption density distribution plots. Most high S MOFs have multiple different metal nodes or other atoms except C, O, and H, such as N and P. A variety of metal nodes and nonmetallic atoms provide more adsorption sites, resulting in high selectivity.

Then, the adsorption behavior with various concentrations of mixtures was simulated, and it was found that the gas component concentrations, especially the molar ratio of H_2 and N_2, had little effect on NH_3 adsorption performance, which had verified the universality of the screening calculations in this work. Finally, we verified the effect of the intrinsic flexibility of MOFs on the adsorption performance. The assumption that MOFs are rigid is feasible in high-throughput computational screening, because the purpose of the screening is to identify a batch of potential MOFs. But the intrinsic flexibility of MOFs should be taken into account when accurate simulations of the adsorption performance are required. The findings obtained in this work not only help to understand the ammonia adsorption behaviors in MOFs but also guide the exploration of MOF adsorbents for efficient ammonia capture from $H_2/N_2/NH_3$ mixtures.

■ ASSOCIATED CONTENT

Supporting Information

The Supporting Information is available free of charge at https://pubs.acs.org/doi/10.1021/acsomega.2c04517.

The Lennard-Jones parameters of MOFs; preliminary screening results for 1709 MOFs; equilibrium calculation results for 195 MOFs; adsorption performance of EKOPIE allowing intrinsic flexibility; input files for all calculations by RASPA 2.0 as well as the input files related to the multiple snapshot approach (PDF)

■ AUTHOR INFORMATION

Corresponding Author

Haiou Wang − *State Key Laboratory of Clean Energy Utilization, Zhejiang University, Hangzhou 310027, P. R. China;* orcid.org/0000-0002-6480-2657; Phone: +86 0571 87951764; Email: wanghaiou@zju.edu.cn.; Fax: +86 0571 87951764

Authors

Zhaofan Zhu − *State Key Laboratory of Clean Energy Utilization, Zhejiang University, Hangzhou 310027, P. R. China;* orcid.org/0000-0002-7730-1376

Xiao-Yu Wu − *Department of Mechanical and Mechatronics Engineering, University of Waterloo, Waterloo, Ontario N2L 3G1, Canada*

Kun Luo − *State Key Laboratory of Clean Energy Utilization, Zhejiang University, Hangzhou 310027, P. R. China;* orcid.org/0000-0003-3644-9400

Jianren Fan − *State Key Laboratory of Clean Energy Utilization, Zhejiang University, Hangzhou 310027, P. R. China;* orcid.org/0000-0002-6332-6441

Complete contact information is available at: https://pubs.acs.org/10.1021/acsomega.2c04517

Notes

The authors declare no competing financial interest.

■ ACKNOWLEDGMENTS

This work was supported by Natural Science Foundation of China (Grant No. 52022091). This work was also supported by the Fundamental Research Funds for the Central Universities. X.Y. Wu was supported by the University of Waterloo Start-up Grant.

■ REFERENCES

(1) Demirhan, C. D.; Tso, W. W.; Powell, J. B.; Pistikopoulos, E. N. Sustainable ammonia production through process synthesis and global optimization. *AIChE J.* **2019**, *65*, No. e16498.

(2) Vikrant, K.; Kumar, V.; Kim, K.-H.; Kukkar, D. Metal−organic frameworks (MOFs): potential and challenges for capture and abatement of ammonia. *J. Mater. Chem. A* **2017**, *5*, 22877−22896.

(3) Martínez-Ahumada, E.; Díaz-Ramírez, M. L.; Velásquez-Hernández, M. d. J.; Jancik, V.; Ibarra, I. A. Capture of toxic gases in MOFs: SO2, H2S, NH3 and NOx. *Chem. Sci.* **2021**, *12*, 6772−6799.

(4) Von Blottnitz, H.; Curran, M. A. A review of assessments conducted on bio-ethanol as a transportation fuel from a net energy, greenhouse gas, and environmental life cycle perspective. *J. Cleaner Prod.* **2007**, *15*, 607−619.

(5) Jain, M.; Muthalathu, R.; Wu, X.-Y. Electrified ammonia production as a commodity and energy storage medium to connect the food, energy, and trade sectors. *iScience* **2022**, *25*, 104724.

(6) Zhou, D.; Zhou, R.; Zhou, R.; Liu, B.; Zhang, T.; Xian, Y.; Cullen, P. J.; Lu, X.; Ostrikov, K. K. Sustainable ammonia production by non-thermal plasmas: Status, mechanisms, and opportunities. *Chem. Eng. J.* **2021**, *421*, 129544.

(7) Zhang, W. Alternative energy sources for green chemistry. *Green Process. Synth.* **2017**, *6*, 131−132.

(8) MacFarlane, D. R.; Cherepanov, P. V.; Choi, J.; Suryanto, B. H.; Hodgetts, R. Y.; Bakker, J. M.; Vallana, F. M. F.; Simonov, A. N. A roadmap to the ammonia economy. *Joule* **2020**, *4*, 1186−1205.

(9) Rouwenhorst, K. H.; Lefferts, L. Feasibility study of plasma-catalytic ammonia synthesis for energy storage applications. *Catalysts* **2020**, *10*, 999.

(10) Duan, G.; Chen, Y.; Tang, Y.; Gasem, K. A.; Wan, P.; Ding, D.; Fan, M. Advances in electrocatalytic ammonia synthesis under mild conditions. *Prog. Energy Combust. Sci.* **2020**, *81*, 100860.

(11) Soloveichik, G. Electrochemical synthesis of ammonia as a potential alternative to the Haber−Bosch process. *Nat. Catal.* **2019**, *2*, 377−380.

(12) Montoya, J. H.; Tsai, C.; Vojvodic, A.; Nørskov, J. K. The challenge of electrochemical ammonia synthesis: a new perspective on the role of nitrogen scaling relations. *ChemSusChem* **2015**, *8*, 2180−2186.

(13) Singh, A. R.; Rohr, B. A.; Schwalbe, J. A.; Cargnello, M.; Chan, K.; Jaramillo, T. F.; Chorkendorff, I.; Nørskov, J. K. Electrochemical Ammonia Synthesis—The Selectivity Challenge. *ACS Catal.* **2017**, *7*, 706−709.

(14) Medford, A. J.; Hatzell, M. C. Photon-driven nitrogen fixation: current progress, thermodynamic considerations, and future outlook. *ACS Catal.* **2017**, *7*, 2624−2643.

(15) Vu, M.-H.; Sakar, M.; Hassanzadeh-Tabrizi, S. A.; Do, T.-O. Photo (electro) catalytic nitrogen fixation: problems and possibilities. *Adv. Mater. Interfaces* **2019**, *6*, 1900091.

(16) Chen, X.; Li, N.; Kong, Z.; Ong, W.-J.; Zhao, X. Photocatalytic fixation of nitrogen to ammonia: state-of-the-art advancements and future prospects. *Mater. Horiz.* **2018**, *5*, 9−27.

(17) Wang, Q.; Guo, J.; Chen, P. Recent progress towards mild-condition ammonia synthesis. *J. Energy Chem.* **2019**, *36*, 25−36.

(18) Chen, J. G.; Crooks, R. M.; Seefeldt, L. C.; Bren, K. L.; Bullock, R. M.; Darensbourg, M. Y.; Holland, P. L.; Hoffman, B.; Janik, M. J.;

Jones, A. K.; et al. Beyond fossil fuel−driven nitrogen transformations. *Science* **2018**, *360*, No. eaar6611.
(19) Peng, P.; Chen, P.; Schiappacasse, C.; Zhou, N.; Anderson, E.; Chen, D.; Liu, J.; Cheng, Y.; Hatzenbeller, R.; Addy, M.; et al. A review on the non-thermal plasma-assisted ammonia synthesis technologies. *J. Cleaner Prod.* **2018**, *177*, 597−609.
(20) Wang, Y.; Craven, M.; Yu, X.; Ding, J.; Bryant, P.; Huang, J.; Tu, X. Plasma-enhanced catalytic synthesis of ammonia over a Ni/Al2O3 catalyst at near-room temperature: insights into the importance of the catalyst surface on the reaction mechanism. *ACS Catal.* **2019**, *9*, 10780−10793.
(21) Rusanov, V. D.; Fridman, A.; Sholin, G. V. The physics of a chemically active plasma with nonequilibrium vibrational excitation of molecules. *Phys.-Usp.* **1981**, *24*, 447.
(22) Lamb, K. E.; Dolan, M. D.; Kennedy, D. F. Ammonia for hydrogen storage; A review of catalytic ammonia decomposition and hydrogen separation and purification. *Int. J. Hydrogen Energy* **2019**, *44*, 3580−3593.
(23) Kang, D. W.; Ju, S. E.; Kim, D. W.; Kang, M.; Kim, H.; Hong, C. S. Emerging porous materials and their composites for NH3 gas removal. *Adv. Sci.* **2020**, *7*, 2002142.
(24) Katz, M. J.; Howarth, A. J.; Moghadam, P. Z.; DeCoste, J. B.; Snurr, R. Q.; Hupp, J. T.; Farha, O. K. High volumetric uptake of ammonia using Cu-MOF-74/Cu-CPO-27. *Dalton Trans* **2016**, *45*, 4150−4153.
(25) Pérez-Pellitero, J.; Pirngruber, G. D. In *New Developments in Adsorption/Separation of Small Molecules by Zeolites*; Valencia, S., Rey, F., Eds.; Springer International Publishing: Cham, 2020; pp 195−225.
(26) Suhas; Carrott, P.; Ribeiro Carrott, M. Lignin − from natural adsorbent to activated carbon: A review. *Bioresour. Technol.* **2007**, *98*, 2301−2312.
(27) Gupta, A. D.; Rene, E. R.; Giri, B. S.; Pandey, A.; Singh, H. Adsorptive and photocatalytic properties of metal oxides towards arsenic remediation from water: A review. *J. Environ. Chem. Eng.* **2021**, *9*, 106376.
(28) Freund, R.; Zaremba, O.; Arnauts, G.; Ameloot, R.; Skorupskii, G.; Dincă, M.; Bavykina, A.; Gascon, J.; Ejsmont, A.; Goscianska, J.; et al. The current status of MOF and COF applications. *Angew. Chem., Int. Ed.* **2021**, *60*, 23975−24001.
(29) Furukawa, H.; Ko, N.; Go, Y. B.; Aratani, N.; Choi, S. B.; Choi, E.; Yazaydin, A. Ö.; Snurr, R. Q.; O'Keeffe, M.; Kim, J.; et al. Ultrahigh porosity in metal-organic frameworks. *Science* **2010**, *329*, 424−428.
(30) Farha, O. K.; Eryazici, I.; Jeong, N. C.; Hauser, B. G.; Wilmer, C. E.; Sarjeant, A. A.; Snurr, R. Q.; Nguyen, S. T.; Yazaydın, A. O.; Hupp, J. T. Metal−organic framework materials with ultrahigh surface areas: is the sky the limit? *J. Am. Chem. Soc.* **2012**, *134*, 15016−15021.
(31) Rezaei, F.; Lawson, S.; Hosseini, H.; Thakkar, H.; Hajari, A.; Monjezi, S.; Rownaghi, A. A. MOF-74 and UTSA-16 film growth on monolithic structures and their CO2 adsorption performance. *Chem. Eng. J.* **2017**, *313*, 1346−1353.
(32) Zhao, X.; Wang, Y.; Li, D.-S.; Bu, X.; Feng, P. Metal−organic frameworks for separation. *Adv. Mater.* **2018**, *30*, 1705189.
(33) Wang, Q.; Astruc, D. State of the art and prospects in metal−organic framework (MOF)-based and MOF-derived nanocatalysis. *Chem. Rev.* **2020**, *120*, 1438−1511.
(34) Lustig, W. P.; Mukherjee, S.; Rudd, N. D.; Desai, A. V.; Li, J.; Ghosh, S. K. Metal−organic frameworks: functional luminescent and photonic materials for sensing applications. *Chem. Soc. Rev.* **2017**, *46*, 3242−3285.
(35) Chedid, G.; Yassin, A. Recent trends in covalent and metal organic frameworks for biomedical applications. *Nanomaterials* **2018**, *8*, 916.
(36) Spanopoulos, I.; Xydias, P.; Malliakas, C. D.; Trikalitis, P. N. A straight forward route for the development of metal−organic frameworks functionalized with aromatic- OH groups: synthesis, characterization, and gas (N2, Ar, H2, CO2, CH4, NH3) sorption properties. *Inorg. Chem.* **2013**, *52*, 855−862.
(37) Kumar, P.; Kim, K.-H.; Kwon, E. E.; Szulejko, J. E. Metal−organic frameworks for the control and management of air quality: advances and future direction. *J. Mater. Chem. A* **2016**, *4*, 345−361.
(38) Khabzina, Y.; Dhainaut, J.; Ahlhelm, M.; Richter, H.-J.; Reinsch, H.; Stock, N.; Farrusseng, D. Synthesis and shaping scale-up study of functionalized UiO-66 MOF for ammonia air purification filters. *Ind. Eng. Chem. Res.* **2018**, *57*, 8200−8208.
(39) Yu, D.; Ghosh, P.; Snurr, R. Q. Hierarchical modeling of ammonia adsorption in functionalized metal−organic frameworks. *Dalton Trans* **2012**, *41*, 3962−3973.
(40) Bobbitt, N. S.; Mendonca, M. L.; Howarth, A. J.; Islamoglu, T.; Hupp, J. T.; Farha, O. K.; Snurr, R. Q. Metal−organic frameworks for the removal of toxic industrial chemicals and chemical warfare agents. *Chem. Soc. Rev.* **2017**, *46*, 3357−3385.
(41) Yuan, X.; Deng, X.; Cai, C.; Shi, Z.; Liang, H.; Li, S.; Qiao, Z. Machine learning and high-throughput computational screening of hydrophobic metal−organic frameworks for capture of formaldehyde from air. *Green Energy Environ* **2021**, *6*, 759−770.
(42) Liu, Z.; Wang, X.; Liu, Y.; Li, L.; Li, S. Computational screening of metal-organic frameworks for ammonia capture from humid air. *Microporous Mesoporous Mater.* **2022**, *331*, 111659.
(43) Nazarian, D.; Camp, J. S.; Sholl, D. S.*Computation-Ready Experimental Metal-Organic Framework (CoRE MOF) 2014 DDEC Database*; 2016; DOI: 10.5281/zenodo.3986573. Yongchul G. Chung (drygchung@gmail.com) maintains this particular dataset but was not involved in deriving the dataset.
(44) Wilmer, C. E.; Leaf, M.; Lee, C. Y.; Farha, O. K.; Hauser, B. G.; Hupp, J. T.; Snurr, R. Q. Large-scale screening of hypothetical metal−organic frameworks. *Nat. Chem.* **2012**, *4*, 83−89.
(45) Groom, C. R.; Bruno, I. J.; Lightfoot, M. P.; Ward, S. C. The Cambridge structural database. *Acta Crystallogr., Sect. B: Struct. Sci., Cryst. Eng. Mater.* **2016**, *72*, 171−179.
(46) Chung, Y. G.; Camp, J.; Haranczyk, M.; Sikora, B. J.; Bury, W.; Krungleviciute, V.; Yildirim, T.; Farha, O. K.; Sholl, D. S.; Snurr, R. Q. Computation-ready, experimental metal−organic frameworks: A tool to enable high-throughput screening of nanoporous crystals. *Chem. Mater.* **2014**, *26*, 6185−6192.
(47) Chung, Y. G.; Haldoupis, E.; Bucior, B. J.; Haranczyk, M.; Lee, S.; Zhang, H.; Vogiatzis, K. D.; Milisavljevic, M.; Ling, S.; Camp, J. S.; et al. Advances, updates, and analytics for the computation-ready, experimental metal−organic framework database: CoRE MOF 2019. *J. Chem. Eng. Data* **2019**, *64*, 5985−5998.
(48) Altintas, C.; Avci, G.; Daglar, H.; Azar, A. N. V.; Erucar, I.; Velioglu, S.; Keskin, S. An extensive comparative analysis of two MOF databases: high-throughput screening of computation-ready MOFs for CH4 and H2 adsorption. *J. Mater. Chem. A* **2019**, *7*, 9593−9608.
(49) Li, W.; Xia, X.; Cao, M.; Li, S. Structure−property relationship of metal−organic frameworks for alcohol-based adsorption-driven heat pumps via high-throughput computational screening. *J. Mater. Chem. A* **2019**, *7*, 7470−7479.
(50) Qiao, Z.; Xu, Q.; Jiang, J. Computational screening of hydrophobic metal−organic frameworks for the separation of H 2 S and CO 2 from natural gas. *J. Mater. Chem. A* **2018**, *6*, 18898−18905.
(51) Altintas, C.; Keskin, S. Role of partial charge assignment methods in high-throughput screening of MOF adsorbents and membranes for CO2/CH4 separation. *Mol. Syst. Des. Eng.* **2020**, *5*, 532−543.
(52) Li, W.; Rao, Z.; Chung, Y. G.; Li, S. The role of partial atomic charge assignment methods on the computational screening of metal-organic frameworks for CO2 capture under humid conditions. *ChemistrySelect* **2017**, *2*, 9458−9465.
(53) Manz, T. A.; Sholl, D. S. Chemically meaningful atomic charges that reproduce the electrostatic potential in periodic and nonperiodic materials. *J. Chem. Theory Comput.* **2010**, *6*, 2455−2468.
(54) Ewald, P. P. Die Berechnung optischer und elektrostatischer Gitterpotentiale. *Ann. Phys.* **1921**, *369*, 253−287.
(55) Rappé, A. K.; Casewit, C. J.; Colwell, K.; Goddard, W. A., III; Skiff, W. M. UFF, a full periodic table force field for molecular

mechanics and molecular dynamics simulations. *J. Am. Chem. Soc.* **1992**, *114*, 10024−10035.
(56) Eggimann, B. L.; Sunnarborg, A. J.; Stern, H. D.; Bliss, A. P.; Siepmann, J. I. An online parameter and property database for the TraPPE force field. *Mol. Simul.* **2014**, *40*, 101−105.
(57) Turner, C. H.; Johnson, J. K.; Gubbins, K. E. Effect of confinement on chemical reaction equilibria: The reactions 2NO = (NO)2 and N2 + 3H2 = 2NH3 in carbon micropores. *J. Chem. Phys.* **2001**, *114*, 1851−1859.
(58) Dubbeldam, D.; Calero, S.; Ellis, D. E.; Snurr, R. Q. RASPA: molecular simulation software for adsorption and diffusion in flexible nanoporous materials. *Mol. Simul.* **2016**, *42*, 81−101.
(59) Widom, B. Some topics in the theory of fluids. *J. Chem. Phys.* **1963**, *39*, 2808−2812.
(60) Willems, T. F.; Rycroft, C. H.; Kazi, M.; Meza, J. C.; Haranczyk, M. Algorithms and tools for high-throughput geometry-based analysis of crystalline porous materials. *Microporous Mesoporous Mater.* **2012**, *149*, 134−141.
(61) Shah, M. S.; Tsapatsis, M.; Siepmann, J. I. Identifying optimal zeolitic sorbents for sweetening of highly sour natural gas. *Angew. Chem.* **2016**, *128*, 6042−6046.
(62) Qiao, Z.; Xu, Q.; Cheetham, A. K.; Jiang, J. High-throughput computational screening of metal−organic frameworks for thiol capture. *J. Phys. Chem. C* **2017**, *121*, 22208−22215.
(63) Ahrens, J.; Geveci, B.; Law, C. In *The Visualization Handbook*; Hansen, C., Johnson, C. R., Eds.; Elsevier, 2004; pp 717−731.
(64) Kajiwara, T.; Higuchi, M.; Watanabe, D.; Higashimura, H.; Yamada, T.; Kitagawa, H. A systematic study on the stability of porous coordination polymers against ammonia. *Chem.—Eur. J.* **2014**, *20*, 15611−15617.
(65) de Lange, M. F.; Verouden, K. J.; Vlugt, T. J.; Gascon, J.; Kapteijn, F. Adsorption-driven heat pumps: the potential of metal−organic frameworks. *Chem. Rev.* **2015**, *115*, 12205−12250.
(66) Liu, Z.; An, G.; Xia, X.; Wu, S.; Li, S.; Wang, L. The potential use of metal−organic framework/ammonia working pairs in adsorption chillers. *J. Mater. Chem. A* **2021**, *9*, 6188−6195.
(67) Peng, P.; Li, Y.; Cheng, Y.; Deng, S.; Chen, P.; Ruan, R. Atmospheric pressure ammonia synthesis using non-thermal plasma assisted catalysis. *Plasma Chem. Plasma Process.* **2016**, *36*, 1201−1210.
(68) Park, J.; Agrawal, M.; Gallis, D. F. S.; Harvey, J. A.; Greathouse, J. A.; Sholl, D. S. Impact of intrinsic framework flexibility for selective adsorption of sarin in non-aqueous solvents using metal−organic frameworks. *Phys. Chem. Chem. Phys.* **2020**, *22*, 6441−6448.
(69) Gee, J. A.; Sholl, D. S. Effect of framework flexibility on C8 aromatic adsorption at high loadings in metal−organic frameworks. *J. Phys. Chem. C* **2016**, *120*, 370−376.
(70) Agrawal, M.; Sholl, D. S. Effects of intrinsic flexibility on adsorption properties of metal−organic frameworks at dilute and nondilute loadings. *ACS Appl. Mater. Interfaces* **2019**, *11*, 31060−31068.
(71) Wilmer, C. E.; Snurr, R. Q. Towards rapid computational screening of metal-organic frameworks for carbon dioxide capture: Calculation of framework charges via charge equilibration. *Chem. Eng. J.* **2011**, *171*, 775−781.
(72) Plimpton, S. Fast parallel algorithms for short-range molecular dynamics. *J. Comput. Phys.* **1995**, *117*, 1−19.
(73) Coupry, D. E.; Addicoat, M. A.; Heine, T. Extension of the universal force field for metal−organic frameworks. *J. Chem. Theory Comput.* **2016**, *12*, 5215−5225.

https://doi.org/10.1021/acsomega.2c04517
ACS Omega 2022, 7, 37640−37653